DSM-Based Precise Pointing Angle Deviation Measurement Method for Beaconless Free Space Optical Communication

Xueyuan Ao, Yansheng Zou, Yang Zou, *Student Member, IEEE*, Qirun Fan, Xiaoxiao Dai, *Member, IEEE*, Chen Liu, Qi Yang, *Senior Member, IEEE*, and Deming Liu

***Abstract*—In free space optical (FSO) communication, acquisition, tracking and pointing (ATP) is the key technology to maintain a high-quality FSO link. Specifically, the detection of pointing angle deviation greatly affects the performance of ATP, especially under weak receiving power. However, the separated beacon laser beam commonly used in ATP will increase the structural complexity of the terminal such as the size, weight, and power. It is unwanted in some limited applications such as satellite. To improve the pointing accuracy with weak signal in beaconless FSO communication, we propose a delta-sigma enabled beaconless cross-correlation (CCR) method with four-quadrant detectors. In the proposed method, a low-frequency sine analog signal for CCR calculation is modulated into a 1-bit digital signal by delta-sigma modulation and then inserted into the communication data as a training sequence. The root means square error (RMSE) of the pointing angle deviation measurement is 14.17 μrad with the incident optical power of −40 dBm. Compared with the direct intensity method, of which RMSE is 67.61 μrad, the proposed method can effectively improve the pointing accuracy with weak power without a beacon laser in FSO communication.**

***Index Terms*—Four-quadrant detector, pointing angle deviation measurement, beaconless free space optical communication, cross-correlation algorithm, delta-sigma modulation.**

I. Introduction

FREE space optical (FSO) communication has always been an attractive technology owing to its unique advantages such as high capacity, inherent security, license-free bandwidth, and easy deployment [1], [2]. However, the FSO communication can be affected by atmospheric attenuation, atmospheric turbulence, pointing error, angle-of-arrival (AOA) fluctuations [3], [4], [5], etc. resulting in fluctuation and reduction of the received optical power. The impact of pointing error and AOA fluctuations on alignment is particularly important owing to the point-to-point transmission mode of spatial laser. Therefore, the technology of acquisition, tracking and pointing (ATP) is usually applied to ensure the well establishment of the FSO links [6], [7]. Among the composing technologies of ATP, the measurement of pointing angle deviation is particularly important for the performance of the entire FSO system. However, inherent background light noise and dark current of four-quadrant detector (4-QD) are hard to ignore, thus most of the position measurement methods [8], [9], [10], [11] cannot be effectively implemented. An accuracy pointing angle deviation measurement method under weak signal is highly required.

Moreover, in some constrained scenarios such as microsatellite, CubeSat, and unmanned aerial vehicles (UAVs), the size, weight, and power (SWaP) of FSO terminals is strictly restricted [12], [13]. Therefore, beaconless FSO communication and alignment, which uses the transmitted signal laser itself as the targeting beacon [14], [15], becomes a trend. The communication and alignment modules can preferably be concentrated on one set of hardware in the FSO terminal which relieves the pressure of SWaP. In this case, the optical power used for alignment is even weaker, and the accuracy of pointing angle deviation measurement will be severely affected. Therefore, a precise-enhanced pointing angle deviation measurement method with simple hardware configuration and power consumption under weak signal is necessary.

In this paper, we propose to apply the CCR algorithm [16], [17], [18] with four-quadrant detectors to improve the measurement accuracy of pointing angle deviation. The CCR algorithm requires the received light to be modulated by a sine signal, which cannot be directly achieved in the beaconless case, because the light carries the communication payload. Therefore, we proposed to utilize delta-sigma modulation (DSM) to convert the analog sine signal into a 1-bit digital signal, which can be simply combined with the communication payload as a training sequence and transmitted together [19], [20], [21]. Then in the receiver, this modulated digital signal can be recovered to the original analog sine signal through simple filtering and be applied in the CCR algorithm to improve the measurement accuracy of pointing angle deviation in beaconless FSO communication. In the experimental demonstration, a low-frequency analog sine signal with 10 MHz used for alignment is firstly

Manuscript received 6 July 2023; revised 5 October 2023; accepted 19 October 2023. Date of publication 23 October 2023; date of current version 6 November 2023. This work was supported in part by the Innovation Fund of WNLO, in part by National Natural Science Foundation of China under Grants 62275091 and 61975064, in part by the Science and Technology Planning Project of Shenzhen Municipality under Grant JCYJ20200109142010888, and in part by Shenzhen Science and Technology Program under Grant GJHZ20210705142539008. *(Corresponding author: Xiaoxiao Dai.)*

The authors are with the School of Optical and Electronic Information, Huazhong University of Science and Technology, Wuhan 430074, China and also with the Research Institute of Huazhong, University of Science and Technology in Shenzhen, Shenzhen 518000, China (e-mail: daixx@hust.edu.cn).

Digital Object Identifier 10.1109/JPHOT.2023.3326844

TABLE I
THE RMSE VALUES OF POINTING ANGLE DEVIATION WITH DIFFERENT METHODS AND OPTICAL POWER

Refs	Scenario	Methods	SNR	δ_{RMSE}/mm
[16]	Weak Power	Cyclic CCR	-14.6	0.0044
[17]	Weak Power	Kalman filtering	-10	0.0049
[18]	Beaconless Weak Power	TRC	-14.6	0.0069
This Work	Beaconless Weak Power	DSM-based CCR	**~-15.6 (-40 dBm)**	**0.0028 (14.17μrad)**

modulated into a 1-bit digital signal by DSM and then inserted into the communication payload as a training sequence. The communication payload is a pseudo-random binary sequence (PRBS) with 1 Gb/s data rate. The two parts are transmitted together in one laser beam. After a 200 mm FSO link in the experiment, the laser beam is focused on the surface of 4-QD and its output is captured by the oscilloscope for further offline processing. The sine signal is recovered simply by low-pass filtering and used to measure the pointing angle deviation with the CCR algorithm. Experimental results show that the root means square error (RMSE) of pointing angle deviation measurement is 14.17 μrad with the incident optical power of -40 dBm. Compared with the direct intensity method, for which RMSE is 67.61 μrad, the proposed method can effectively improve the measurement accuracy with weak power in beaconless FSO communication. We compared the existing methods under weak power [16], [17], [18] with our proposed DSM-based CCR method in Table I. Since different methods are used for improving the measurement accuracy of pointing angle deviation, the values of RMSE of angle deviation are different under different signal-to-noise ratio (SNR). With similar optical power (or output SNR of 4-QD), the proposed method has a better performance in pointing angle deviation measurement due to the higher in-band SNR of DSM. Additionally, a communication experiment with 1 Gb/s payload is also illustrated on the basis of alignment. Under the 7% forward error correction (FEC) limit, the receiving sensitivity is −38 dBm.

II. PRINCIPLE

A. DSM-Based Pointing Angle Deviation Measurement Scheme

Fig. 1 presents the terminal structure of the proposed DSM-based pointing angle deviation measurement scheme for beaconless FSO communication. The red and blue lines represent the path of the transmitted and received laser, respectively. In the transmitter shown in Fig. 1(a), the generated signal consists of two parts: one is the communication payload, and the other is used as the characteristic signal to improve the measurement accuracy of pointing angle deviation by CCR algorithm. Noteworthy, the characteristic signal of low-frequency analog sine is not directly inserted into the transmitted data. By DSM, the analog sine is converted into 1-bit sequence matching the

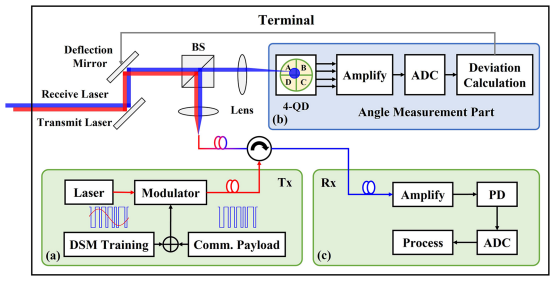

Fig. 1. Terminal structure of the proposed DSM-based pointing angle deviation measurement scheme for beaconless FSO communication.

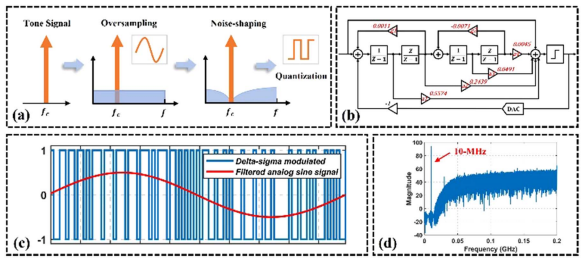

Fig. 2. (a) Processes of DSM technology; (b) a four-order delta-sigma modulator based on CRFF structure; (c) analog sine signal and its corresponding delta-sigma modulated signal; (d) signal spectrum after DSM.

communication rate and combined with the data as a training sequence. They can be transmitted directly through the transceiver ports without digital-to-analog converters (DACs), which can reduce the complexity of the FSO terminal. Moreover, frequency of the sine wave can be flexibly adjusted by DSM to adapt to some special scenarios such as bandwidth-limited systems. The combined signal is then sent to the modulator and modulated into the optical carrier. After passing through the circulator, the laser beam is collimated and reflected, and then enters the free space for transmission.

For the received laser beam, it is divided into two branches by a beam splitter (BS) for alignment and communication, as shown in Fig. 2(b) and (c) respectively. For alignment, the beam is focused on the 4-QD by imaging lens and received by 4-QD. The output intensity of 4-QD is amplified and then sampled by analog-to-digital converters (ADCs). In this process, the original analog sine wave can be easily recovered from the DSM training sequence by low-pass filtering. The recovered sine signal is then processed by CCR algorithm to measure the pointing angle deviation, which is more accurate than the direct intensity method only with the 4-QD output. Meanwhile, the other beam is coupled into the fiber and used for communication. Similarly, through low-pass filtering, the DSM training sequence and communication payload can also be simply separated. In order to better understand the proposed scheme, the principles of DSM and the CCR algorithm of 4-QD are explained in detail as follows.

B. Principle of Delta-Sigma Modulation

Fig. 2(a) shows the processes of DSM. Firstly, the analog signal is oversampled to expand its Nyquist zone. The quantization noise will be evenly distributed over a wider frequency

range. Then, the noise shaping technique pushes most of the quantization noise out of the signal band, leaving trivial residual noise. After 1-bit quantization, the analog signal will be converted into 1-bit digital signal with the sampling rate of the DSM, as shown in Fig. 2(c). Finally, the originally analog signal can be reconstructed from the 1-bit digital signal through simple filtering. The DSM modulator with four-order cascade-of-resonators feedforward (CRFF) structure used in this work is shown in Fig. 2(b), and the noise transfer function (NTF) and signal transfer function (STF) of it are as follows [19], [20], [21]:

$$\begin{aligned} \frac{1}{NTF} &= 1 + \frac{a_1(z-1)+a_2 z}{(z-1)^2 + g_1 z} \\ &\quad + \frac{[a_3(z-1)+a_4 z]z}{[(z-1)^2 + g_1 z][(z-1)^2 + g_2 z]} \\ z &= \mathrm{e}^{\frac{j2\pi f}{f_s}} \\ STF &= 1 \end{aligned} \tag{1}$$

where a_1-a_4, g_1-g_2 are the feedback coefficients of each node of the delta-sigma modulator, f_s represents the sampling rate of DSM, f represents the variable frequency of analog signal and $f \in [0,\ f_s/2]$. By adjusting the feedback coefficients, the zero point of NTF can be arbitrarily changed to match different frequencies of the analog signals. Setting $f = 10$ MHz and $f_s = 1$ GHz, the feedback coefficients have been indicated in Fig. 2(b). Signal spectrum after DSM is shown in Fig. 2(d). The quantization noise is pushed away from the 10 MHz frequency point, bringing in a higher SNR.

C. Cross-Correlation-Based SNR Enhancement for 4-QD

4-QD consists of four identical p-n junction photodiodes named four quadrants (A, B, C, D), as shown in the 4-QD module in Fig. 1(b). When the laser beam is focused on the 4-QD surface, each quadrant can output the amplitude of photocurrent independently, which can be used to calculate the laser spot position. Setting $I_{A,B,C,D}$ as the output photocurrent of different quadrants respectively, the position of the centroid laser spot on the 4-QD along the x-axis and y-axis can be expressed as follows [22], [23]:

$$\begin{aligned} x &= x_0 + k \cdot \Delta x = x_0 + k \cdot \frac{(I_A + I_D) - (I_B + I_C)}{I_A + I_B + I_C + I_D} \\ y &= y_0 + k \cdot \Delta y = y_0 + y \cdot \frac{(I_A + I_B) - (I_C + I_D)}{I_A + I_B + I_C + I_D} \end{aligned} \tag{2}$$

where $[x_0, y_0]$ is the central position of 4-QD, k is a constant value related to the size of the laser spot and optical intensity distribution which can be obtained by the calibration test. From (2), the position deviation of the received laser beam is obtained and used to feedback the deflection mirror for alignment. This is the direct intensity method usually used in 4-QD. However, the output photocurrent of 4-QD is not entirely from the received laser beam. Background light and dark current are also part of it. Therefore, assuming that each quadrant of 4-QD is affected by the same sources, the compensated output photocurrent of each quadrant can be expressed as follow:

$$I_n^* = I_n + I_{back} + I_{dark} \tag{3}$$

where n represents the corresponding quadrant, I_{back} is response of the background light and I_{dark} is response of the dark current. Taking the x-axis as an example, setting $I_{QD} = I_A + I_B + I_C + I_D$, the calculated error can be expressed as follows:

$$\begin{aligned} x^* - x &= x_0 - x_0 + k \cdot (\Delta x^* - \Delta x) \\ &= k \cdot \left(\frac{I_A + I_D - I_B - I_C}{I_{QD} + I_{back} + I_{dark}} - \frac{I_A + I_D - I_B - I_C}{I_{QD}} \right) \\ &= -k \cdot \frac{I_A + I_D - I_B - I_C}{I_{QD}} \cdot \frac{I_{back} + I_{dark}}{I_{QD} + I_{back} + I_{dark}} \end{aligned} \tag{4}$$

It can be seen from (4) that I_{back} and I_{dark} will affect the calculation results of position deviation. When I_{QD} is large enough, the influence of background light and dark current is small. However, when the received signal is extremely weak after the FSO transmission, the impact will become obvious and the measurement precision is greatly deteriorated. The CCR algorithm is effective in improving the measurement precision under weak receiving power [10]. In this way, a typical low-frequency sine signal is modulated to the alignment laser. The output of the 4-QD can be expressed as $V_n(t)$:

$$V_n(t) = A_n \sin(2\pi f t + \varphi) + N_n(t) \tag{5}$$

where f represents the frequency of modulated sine signal, A_n represents the output intensity of each quadrant, $N_n(t)$ represents the other noise such as background light and dark current. In the receiver, the correlated sine signal $S_n(t)$ with the same frequency as the transmitter is generated. It can be written as:

$$S_n(t) = B \sin(2\pi f t + \theta) \tag{6}$$

where B represents the intensity of the correlated signal. The correlation operation of $V_n(t)$ and $S_n(t)$ can be expressed as:

$$\begin{aligned} R_n &= \frac{1}{T} \int_0^T V_n(t) S_n(t)\, dt \\ &= \frac{A_n B}{2} \cos(\varphi - \theta) - \frac{A_n B}{2T} \int_0^T \cos(4\pi f + \varphi + \theta) dt \\ &\quad + \frac{B}{T} \int_0^T N_n(t) \sin(2\pi f + \theta) dt \end{aligned} \tag{7}$$

where T represents the length of CCR data. When T is large enough, $\lim_{T\to\infty} \frac{A_n B}{2T} \int_0^T \cos(4\pi f + \varphi + \theta) dt \approx 0$, and the second component of R_n is close to 0 and can be ignored. Additionally, since the noise $N_n(t)$ is independent of the CCR data, the third component of R_n is also small enough to be neglected. The result of correlation operation of R_n can be expressed as:

$$R_n \approx \frac{A_n B}{2} \cos(\varphi - \theta) \tag{8}$$

Therefore, only the components that correlate with the $S_n(t)$ could pass through the correlator, and the other noise will be suppressed. Controlling the phase θ to make $\varphi - \theta = 0$, a

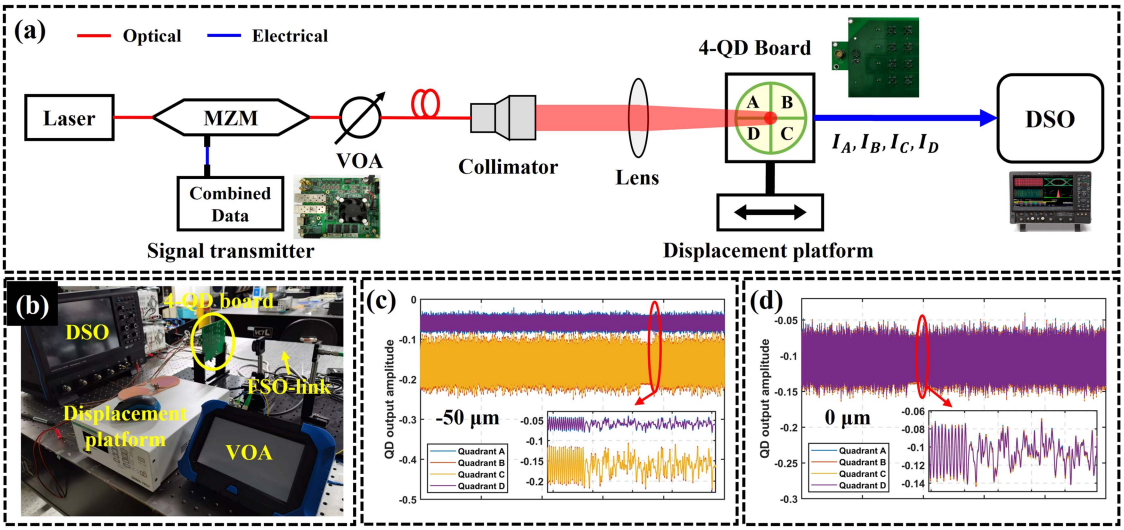

Fig. 3. (a) Experimental setup of the proposed scheme; (b) experimental scene; (c) time domain waveforms of 4-QD output with -50 μm offset; (d) time domain waveforms of 4-QD output with 0 μm offset.

biggest amplitude value $A_n B/2$ can be obtained. Substituting the I_n by the correlation value R_n in (2), a more precise position of the beam spot centroid on the detector can be obtained.

III. Experiment Setup

Experimental setup of the proposed DSM-based pointing angle deviation measurement scheme is shown in Fig. 3(a). The red and blue lines in the diagram represent the transmission link of optical and electrical signals, respectively. In the transmitter, a narrow-linewidth tunable laser is used as the source to generate the continuous laser and its wavelength is set as 1550 nm. The generated laser is then injected into a Mach-Zehnder modulator (MZM) for modulation. Noteworthy, the low-frequency sine signal with 10 MHz for pointing angle deviation measurement is shaped by the DSM and converted into a 1 Gb/s 1-bit sequence which combined with the communication data (PRBS with 1 Gb/s data rate) as a training sequence. The joint digital signal is stored in the random-access memory (RAM) of the field programmable gate array (FPGA, XC7K325T-FFG676-2I) and then coupled to the MZM input only through the digital port instead of DACs. Subsequently, the modulated optical signal out of MZM is attenuated by a variable optical attenuator (VOA) to different optical powers to simulate the attenuation in the practical FSO scenario. The DC-bias used for MZM is set near the linear bias point (Quadrature Point, approximately 3.5 V) to ensure that the transmission signal is effectively modulated. Afterwards, the attenuated optical signal is coupled into a collimator and launched into the FSO link for transmission.

Through 200 mm FSO link on the experimental station, the laser beam is focused on the 4-QD surface by an imaging lens with 200 mm focal length in the receiver. At a suitable position in front of the focus of the lens, the surface of the 4-QD (G6849-01, Hamamatsu) is located. Noteworthy, a self-developed 4-QD board is applied in this experiment, which integrates the 4-QD device and subsequent amplification circuit. The output of 4-QD board is the result after amplification with sufficient gain. The 4-QD board is installed on a two-dimensional precision displacement platform (FC-611, Sigma Technology) with minimum displacement distance of 5 nm to simulate the position deviation of the practical laser spot (along the x-axis). Finally, the output of the 4-QD board is captured by a digital sampling oscilloscope (DSO, LeCroy WaveRunner8404M) with 500 MHz sampling frequency and 1 M points sampling depth for later pointing deviation calculation. The practical scene of the experiment is shown in Fig. 3(b).

For the DSM-based CCR scheme, the DSM modulated sine signal can be simply distinguished and recovered by low-pass filtering in the receiver. As a comparison, the output amplitude of 4-QD will also be used to measure the pointing angle deviation by the direct intensity method. Adjusting the incident optical power from -20 to -50 dBm by VOA with steps of 5 dBm, the measurement effect under different FSO attenuation is obtained. Noteworthy, the data of the max incident optical power of -20 dBm is used to calibrate the value of k in (2). Additionally, since this work only discusses the measurement of the pointing angle deviation under low optical power, the influence of nonlinear region of 4-QD is not considered. Therefore, to ensure that the data collected in the experiment falls within the linear region of the 4-QD receiving surface, the laser spot has been controlled in a relatively conservative range. The 4-QD board installed on the displacement platform will move from -50 to $+50$ μm with steps of 5 μm in the x-axis to simulate the offset of laser spot.

Fig. 3(c) and (d) show the output time-domain waveforms of 4-QD quadrants captured by the DSO when the position of displacement platform is set as -50 and 0 μm, respectively. In the zoomed-in part of these figures, the sine wave modulated by DSM can be recovered directly for subsequent procedures via low-pass filtering, while the communication data with high rate can be truncated and clearly removed. Additionally, as shown in Fig. 3(c), the output of quadrant B and C is equal but greater than quadrant A and D. This means that the spot position on the 4-QD surface is offset from the center in the X-axis direction. As shown in Fig. 3(d), outputs of the four quadrants are the

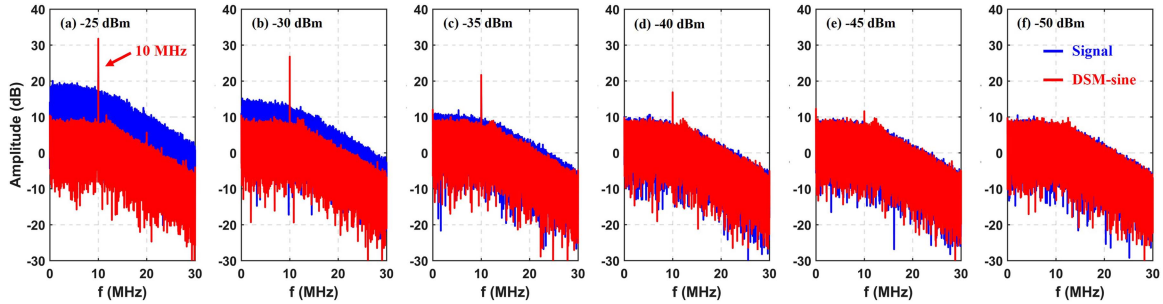

Fig. 4. Spectrum of the received signal and DSM sine wave with different incident optical power. (a) −25 dBm; (b) −30 dBm; (c) −35 dBm; (d) −40 dBm; (e) −45 dBm; (f) −50 dBm.

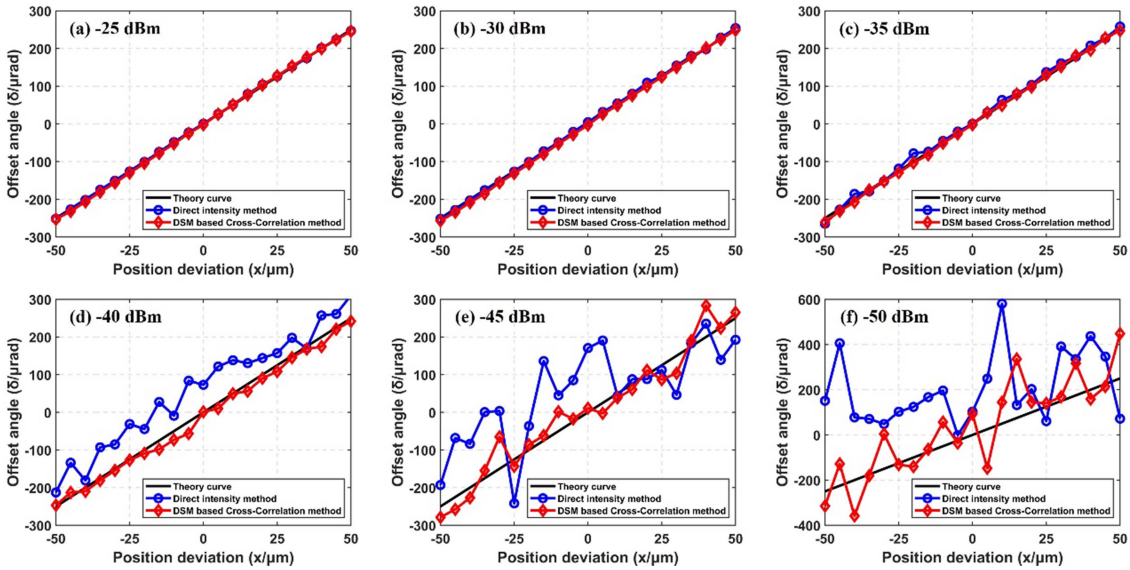

Fig. 5. Experimental comparison between the direct intensity method and the proposed method at different incident optical power. (a) −25 dBm; (b) −30 dBm; (c) −35 dBm; (d) −40 dBm; (e) −45 dBm; (f) −50 dBm.

same, which means that the laser spot is aligned at the center of the 4-QD surface. By comparing the calculated position with the actual ideal position, the pointing angle deviation under different situations can be obtained.

IV. Results and Analysis

A. Pointing Angle Deviation Measurement

By changing the incident optical power with VOA, the output data from 4-QD can be obtained under different attenuation scenarios. With incident optical power from −25 dBm to −50 dBm, the output SNR values of 4-QD are 13.8 dB, 4.1 dB, −6.0 dB, −15.6 dB, −24.2 dB and −25.2 dB respectively. The SNR value is very small when the incident optical power is very low such as -15.6 dB with incident optical power of −40 dBm. Through low-pass filtering, the spectrums of the incomplete signal (blue) and recovered 10 MHz sine signal (red) with different optical power are shown in Fig. 4. When the incident optical power decreases to −35 dBm or even lower, the signal may submerge in the background noise. As for the recovered DSM sine signal, it can play a certain role in amplification while the incident optical power decreases to even -45 dBm. Noteworthy, the spectrum of the DSM sine in Fig. 4 is different from that in Fig. 2(d) which shows the spectrum of the 1-bit digital signal after DSM including the entire bandwidth.

After calibrating the value k in (2) with the incident optical power of −20 dBm, the position of laser spot under different attenuation can be calculated subsequently. With the practical moving distance of the displacement platform from −50 to 50 μm and the imaging lens with a focal length of 200 mm, the pointing angle deviation of laser beam can be obtained in different scenarios. Then, with incident optical power from −25 dBm to −50 dBm, the comparison of pointing angle deviation measurements between the two methods and the practical displacement are shown in Fig. 5(a)–(f) respectively. When the incident optical power is greater than -30 dBm, as shown in Fig. 5(a) and (b), the measurement results of the pointing angle deviation from the two methods are close and consistent with the theoretical values. Since the incident optical power is large enough to suppress the influence of the background noise and dark current. However, when the incident optical power is less than -30 dBm and gradually decreases, the proportion of background noise and dark current in the output of 4-QD cannot be to ignore. As shown in Fig. 5(c)–(f), the measurement

TABLE II
MAXIMUM AND RMSE VALUES OF ANGLE DEVIATION WITH DIFFERENT INCIDENT OPTICAL POWER

Incident Optical Power(dBm)	$\delta_{MAX}(\mu rad)$		$\delta_{RMSE}(\mu rad)$	
	Direct	Proposed	Direct	Proposed
-25	4.23	6.96	1.91	3.78
-30	9.41	10.06	4.06	4.58
-35	22.02	10.41	8.92	4.81
-40	**108.76**	**31.56**	**67.61**	**14.17**
-45	211.09	84.86	111.03	35.24
-50	630.87	261.13	267.65	110.20

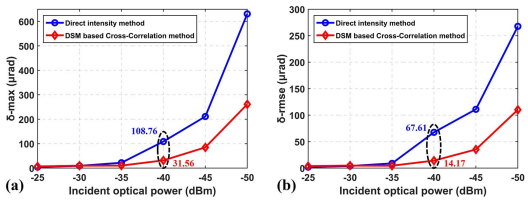

Fig. 6. (a) Maximum of the pointing angle deviation with different optical power; (b) RMSE of the pointing angle deviation with different optical power.

results of pointing angle deviation with direct intensity method are more severely affected by the background noise, resulting in significant errors and fluctuations. For the proposed method, it is obviously smoother and fits the practical curve under weaker power of lower to -45 dBm.

Furthermore, to clearly demonstrate the differences between the two methods, the maximum and RMSE values of the pointing angle deviation (δ_{MAX} and δ_{RMSE}) in the linear region with both methods under different incident optical power are calculated and summarized in Table II. The angle deviation vs. incident optical power curves are also illustrated in Fig. 6. When the incident optical power is sufficient (higher than -35 dBm), the results of both methods are similar to the theoretical values. When the incident optical power drops to -40 dBm, the RMSE value of the direct intensity method increases to 67.61 μrad while the RMSE value of the proposed method is 14.17 μrad. Their maximum values are 108.76 μrad and 31.56 μrad. Obviously, the proposes DSM-based CCR method performs better under weak signals. Its performance will gradually deteriorate when the incident optical power is close to -45 dBm, which is also consistent with the spectrums performance shown in Fig. 4.

B. Communication Test

An additional optical path is supplemented through the BS for communication test based on laser beam alignment. The supplementary experiment diagram is illustrated in Fig. 1(c). On the communication side, as the spatial laser beam is coupled into the fiber, the signal is amplified and then detected by a photo diode detector (PD). The electrical signal output from PD is captured by a DSO and processed offline in MATLAB. In offline data processing, the communication payload and the DSM training can be simply separated. The BER performance of communication payload versus the received optical power (ROP) is shown in Fig. 7. The BER reaches the 7% forward error

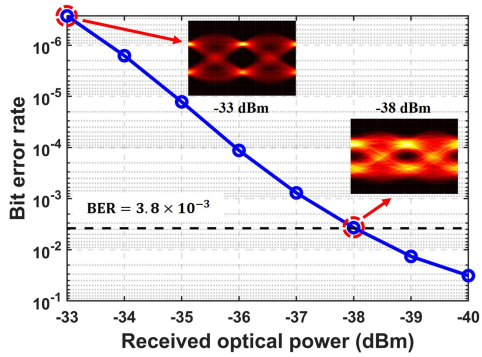

Fig. 7. BER results versus the received optical power, and eye diagrams of the received signals.

correction threshold (BER $= 3.8\times10^{-3}$) with ROP of -38 dBm. Additionally, the eye diagrams of communication payload at the ROP of -33 dBm and -38 dBm are also attached in Fig. 7. The proposed scheme can effectively combine FSO communication and alignment while the received signal is weak. Additionally, the BER performance evaluation in Fig. 7 is completed under the premise of laser beam alignment, and the result of pointing angle deviation measurement is not considered. It is used to verify the communication function of the experimental system as a supplementary test.

V. CONCLUSION

In this paper, we experimentally demonstrate a precise pointing angle deviation measurement scheme for beaconless FSO communication. Based on the DSM-enabled CCR algorithm, a 10 MHz analog sine signal is modulated into a 1-bit digital signal and inserted into the 1 Gb/s PRBS communication data as training signal. In the receiver, the sine signal is recovered by low-pass filtering and used to calculate the pointing angle deviation with the CCR. When the incident optical power is -40 dBm, RMSE of the proposed method is 14.17 μrad, exhibiting much higher accuracy than the traditional direct intensity method, RMSE of which is 67.61 μrad with weak power in beaconless FSO communication. Additionally, under the premise of alignment, the 1 Gb/s payload is transmitted in the communication link with -38 dBm sensitivity under 7% FEC limited.

REFERENCES

[1] M. A. Khalighi and M. Uysal, "Survey on free space optical communication: A communication theory perspective," *IEEE Commun. Surveys Tut.*, vol. 16, no. 4, pp. 2231–2258, Fourth Quarter 2014.
[2] P. Singhal, P. Gupta, and P. Rana, "Basic concept of free space optics communication (FSO): An overview," in *Proc. Int. Conf. Commun. Signal Process.*, 2015, pp. 0439–0442.
[3] G. Xu, N. Zhang, M. Xu, Z. Xu, Q. Zhang, and Z. Song, "Outage probability and average BER of UAV-assisted dual-hop FSO communication with amplify-and-forward relaying," *IEEE Trans. Veh. Technol.*, vol. 72, no. 7, pp. 8287–8302, Jul. 2023.
[4] M. T. Dabiri, S. M. S. Sadough, and I. S. Ansari, "Tractable optical channel modeling between UAVs," *IEEE Trans. Veh. Technol.*, vol. 68, no. 12, pp. 11543–11550, Dec. 2019.
[5] M. T. Dabiri, S. M. S. Sadough, and M. A. Khalighi, "Channel modeling and parameter optimization for hovering UAV-based free-space optical links," *IEEE J. Sel. Areas Commun.*, vol. 36, no. 9, pp. 2104–2113, Sep. 2018.

[6] Z. Xin, Z. Hu, Z. Song, S. Tong, H. Song, and H. Jiang, "Modeling of fine tracking sensor for free space laser communication systems," in *Proc. Symp. Photon. Optoelectron.*, 2009, pp. 1–4.
[7] W. Guanghui, P. Shum, X. Guoliang, and Z. Xuping, "Position detection improvement of position sensitive detector (PSD) by using analog and digital signal processing," in *Proc. 6th Int. Conf. Inf., Commun. Signal Process.*, 2007, pp. 1–4.
[8] D. Li and S. Liu, "Research on four-quadrant detector and its precise detection," *Int. J. Digit. Content Technol. Appl.*, vol. 5, no. 4, pp. 138–143, Apr. 2011.
[9] K. Diao, X. Liu, Z. Yao, W. Lu, and W. Yang, "Improved calibration method of a four-quadrant detector based on Bayesian theory in a laser auto-collimation measurement system," *Appl. Opt.*, vol. 61, no. 19, pp. 5545–5551, 2022.
[10] X. Wang, X. Su, G. Liu, J. Han, W. Zhu, and Z. Liu, "Method to improve the detection accuracy of quadrant detector based on neural network," *IEEE Photon. Technol. Lett.*, vol. 33, no. 22, pp. 1254–1257, Nov. 2021.
[11] Z. Qiu, W. Jia, X. Ma, B. Zou, and L. Lin, "Neural-network-based method for improving measurement accuracy of four-quadrant detectors," *Appl. Opt.*, vol. 61, no. 8, pp. F9–F14, 2022.
[12] H. Arora and R. Goyal, "A review on inter-satellite link in inter-satellite optical wireless communication," *J. Opt. Commun.*, vol. 38, no. 1, pp. 63–67, Apr. 2017.
[13] C. Wang et al., "Pointing and tracking errors due to low-frequency deformation in inter-satellite laser communication," *J. Modern Opt.*, vol. 66, no. 4, pp. 430–437, Feb. 2018.
[14] B. Smutny et al., "5.6 Gbps optical intersatellite communication link," *Proc. SPIE*, vol. 7199, Feb. 2009, Art. no. 719906.
[15] M. Gregory, F. Heine, H. Kämpfner, R. Meyer, R. Fields, and C. Lunde, "TESAT laser communication terminal performance results on 5.6 Gbit coherent inter satellite and satellite to ground links," *Proc. SPIE*, vol. 10565, Nov. 2017, Art. no. 105651F.
[16] Q. Li, S. Xu, J. Yu, L. Yan, and Y. Huang, "An improved method for the position detection of a quadrant detector for free space optical communication," *Sensors*, vol. 19, no. 1, Jan. 2019, Art. no. 175.
[17] J. Yu et al., "High-precision light spot position detection in low SNR condition based on quadrant detector," *Appl. Sci.*, vol. 9, no. 7, Mar. 2019, Art. no. 1299.
[18] Q. Li et al., "TRC-based high-precision spot position detection in inter-satellite laser communication," *Sensors*, vol. 20, no. 19, Oct. 2020, Art. no. 5649.
[19] J. Wang, Z. Jia, L. A. Campos, and C. Knittle, "Delta-sigma modulation for next generation fronthaul interface," *J. Lightw. Technol.*, vol. 37, no. 12, pp. 2838–2850, Jun. 2019.
[20] L. Zhong et al., "An SNR-improved transmitter of delta-sigma modulation supported ultra-high-order QAM signal for fronthaul/WiFi applications," *J. Lightw. Technol.*, vol. 40, no. 9, pp. 2780–2790, May 2022.
[21] X. Ao et al., "Real-time experimental demonstration of hybrid FSO/wireless transmission based on coherent detection and delta-sigma modulation," *IEEE Photon. J.*, vol. 14, no. 6, Dec. 2022, Art. no. 7359908.
[22] J. Zhang et al., "Improved algorithm for expanding the measurement linear range of a four-quadrant detector," *Appl. Opt.*, vol. 58, no. 28, pp. 7741–7748, 2019.
[23] J. Zhang et al., "A calibration and correction method for the measurement system based on four-quadrant detector," *Optik*, vol. 204, Feb. 2020, Art. no. 164226.